



# Mononuclear late first row transition metal complexes of *ONO* donor hydrazone ligand: Synthesis, characterization, crystallographic insight, *in vivo* and *in vitro* anti-inflammatory activity



Umashri Kendur<sup>a</sup>, Geeta H. Chimmalagi<sup>a</sup>, Sunil M. Patil<sup>a</sup>, Kalagouda B. Gudasi<sup>a,\*</sup>, Christopher S. Frampton<sup>b</sup>, Chandrashekhara V. Mangannavar<sup>c</sup>, Iranna S. Muchchandi<sup>c</sup>

<sup>a</sup> Department of Studies in Chemistry, Karnatak University, Dharwad, 580003, Karnataka, India

<sup>b</sup> Institute of Materials & Manufacturing, Wolfson Centre for Materials Processing, Brunel University, London, Uxbridge, United Kingdom

<sup>c</sup> H.S.K. College of Pharmacy, Bagalkot, 587101, Karnataka, India

## ARTICLE INFO

### Article history:

Received 13 July 2017

Received in revised form

5 October 2017

Accepted 6 October 2017

Available online 9 October 2017

### Keywords:

*E*-2-amino-*N'*-(1-(2-hydroxy-6-methyl-4-oxo-4H-pyran-3-yl)ethylidene)benzohydrazide

Transition metal complexes

Single crystal X-ray diffraction study

Mono-deprotonated and doubly

deprotonated

Hirshfeld surface analysis

Anti-inflammatory activity

## ABSTRACT

Air and moisture stable coordination compounds of late first row transition metal ions, viz., Co(II), Ni(II), Cu(II) and Zn(II) with a newly designed ligand, (*E*)-2-amino-*N'*-(1-(2-hydroxy-6-methyl-4-oxo-4H-pyran-3-yl)ethylidene)benzohydrazide ( $H_2L$ ) were prepared and extensively characterized using various spectro-analytical techniques. The ligand acts both in mono as well as doubly deprotonated manner. The ligand to metal stoichiometry was found to be 1:2 in case of complexes using chloride salts, whereas 1:1 in case of copper (II) complex using its acetate salt. The molecular structures of  $H_2L$ , nickel and copper complexes were unambiguously determined by single-crystal X-ray diffraction studies reveal that  $H_2L$  exists in a zwitterionic form while copper complex has copper centre in a distorted square planar environment. On the other hand, cobalt, nickel and zinc complexes display distorted octahedral coordination around the metal ion. In case of  $[Ni(HL)_2] \cdot H_2O$ , intramolecular C–H $\cdots\pi$  stacking interaction were observed between the centroid of five membered chelate ring and phenyl proton C5–H5 and intermolecular C–H $\cdots\pi$  stacking interaction between the centroid of phenyl ring, dehydroacetic acid (DHA) ring and phenyl protons. The  $[Cu(L)DMF]$  complex is stabilized by intramolecular hydrogen bonding N1H $\cdots$ N2 and by intermolecular hydrogen bonding N1H $\cdots$ O4. Intermolecular interactions were investigated by Hirshfeld surfaces. Further,  $H_2L$  and its metal complexes were screened for their *in vivo* and *in vitro* anti-inflammatory activities. The activity of the ligand has enhanced on coordination with transition metals. The tested compounds have shown excellent activity, which is almost equipotent to the standard used in the study.

© 2017 Elsevier B.V. All rights reserved.

## 1. Introduction

The coordination chemistry of *N*-acyl hydrazone (NAH) ligands has captivated considerable assiduity in past few decades, due to their chelating capability, structural flexibility, variable bonding modes towards transition metal ions and a wide range of biological applications [1–4]. NAH has also been used as the bedrock for designing new analgesic and anti-inflammatory compounds, because the NAH subunit is a primal pharmacophore for binding to and inhibiting cyclooxygenases (COXs) [5]. A number of transition metal complexes of NAH have been reported to exhibit DNA

interactions, as well as antimicrobial and antitumor properties [6,7,8a]. The biological activity associated with these compounds is attributed to the presence of –CONHN=CH– moiety. On coordination, the activity of hydrazone increases. Moreover, coordination suppresses the polarity of the metal ion because of the partial sharing of its positive charge with the donor atom inside the chelate ring system, formed during coordination. This process consecutively increases the lipophilic nature of the central metal atom/ion, which in turn favours its pervasion more efficiently through the lipid layers of the microorganism [8b,c].

Further, transition metal complexes of NAH have also shown high catalytic activities in various chemical reactions, to name a few, epoxidation of olefins [9,10], polymerization of ethylene [11], and transamidation of carboxamides with amines [12], etc. Aggoun

\* Corresponding author.

E-mail address: [drkbgudasi@kud.ac.in](mailto:drkbgudasi@kud.ac.in) (K.B. Gudasi).

et al., described the electrocatalytic behaviour of the copper complex of hydrazone ligand prepared by condensation of dehydroacetic acid on 1,2-diaminopropane towards electro-reduction of alkyl and aryl halides [13].

Dehydroacetic acid (DHA), a pyranone derivative is a herculean material which is involved in the synthesis of many heterocyclic compounds. It is prepared by the base-catalyzed (tert-amines; imidazole; 1,4-diazabicyclo[2.2.2]octane (DABCO); pyridine) dimerization of diketene. These compounds have occupied a dominating position in coordination chemistry that explores therapeutic and pharmacological activities [14,15]. Studies on metal chelates with Schiff base of dehydroacetic acid have been reported due to their excellent chelating capacity in modern coordination chemistry. Recently, Edward et al., reported the design and synthesis of a novel class of diaryl heterocyclic with a central six-membered lactone (pyran-2-one) ring which exhibited good *in vitro* COX-2 inhibitory potency and selectivity [16a–h]. Cobalt, nickel, copper and zinc being bio-essential elements, it is conceived that their complexes may find more applications in numerous biological processes [17].

Considering the above-mentioned facts and in continuation of our ongoing research on the study of pharmacological properties of transition metal complexes, the present work was undertaken as an attempt to explore the structural relationship of DHA derived hydrazone with late first row transition metals. Here we report the synthesis and characterization of the DHA derived ligand, its transition metal complexes. A preliminary screening for *in vivo* and *in vitro* anti-inflammatory activity of these new compounds was also studied.

## 2. Experimental

### 2.1. General procedures

All the reagents used in this study were purchased from Sigma Aldrich and used as rendered. The synthesis of precursor, *o*-aminobenzoylhydrazide the precursor was synthesized according to the procedure reported earlier [18,19]. Infrared spectra of the ligand and its metal complexes were recorded in the region 4000–400  $\text{cm}^{-1}$  on a Nicolet 170 SX FT-IR spectrometer (KBr disc matrix). The  $^1\text{H}$  NMR and  $^{13}\text{C}$  NMR spectra were recorded on a Bruker AV400 II spectrometer at 400 MHz in  $\text{DMSO}-d_6/\text{CDCl}_3$  at room temperature using TMS as an internal reference. All the compounds were analyzed for carbon, hydrogen and nitrogen using a Thermo quest elemental analyzer and metal complexes were analyzed for their metal content by standard methods [20]. The UV–Vis spectra of all the compounds in DMF were recorded on a Varian Cary 50 Bio UV–Vis spectrophotometer. Thermograms of the metal complexes were recorded in nitrogen atmosphere on a SDT Q600 Analyzer, keeping the final temperature at 1000 °C with a heating rate of 10 °C/min heating rate. The molar conductivity measurements of 1 mM solutions in DMF were carried out on equiptronics EQ-665 conductivity bridge. EPR spectra were recorded both at room temperature (300 K) and liquid nitrogen temperature (77 K) on a Varian E-112 X-band spectrometer using TCNE (tetracyanoethylene) as 'g' marker ( $g = 2.00277$ ) at a frequency of 9.65 GHz under the magnetic strength of 3000 G. The EI mass spectrum of the ligand was obtained with a Shimadzu GCMS-QP2010S spectrometer. The ESI mass spectral data for all the complexes were obtained from Agilent Technologies India Pvt. Ltd. The X-ray diffraction data of nickel complex were collected at 293 K on a Bruker SMART APEX2 CCD area-detector diffractometer using a graphite monochromator  $\text{Mo}-\text{K}\alpha$  ( $\lambda = 0.71073 \text{ \AA}$ ) radiation source. The frames were integrated with the Bruker SAINT Software package using a narrow-frame algorithm. In the absence of anomalous scattering, Friedel pairs were merged. The H atoms were all located

in a difference map, but those attached to carbon atoms were repositioned geometrically. The H atoms were initially refined with soft restraints on the bond lengths and angles to regularize their geometry, after which the positions were refined with riding constraints [21]. All non-hydrogen atoms were refined anisotropically. Structure solution and refinement were performed using Crystals [22]. Molecular graphics were generated using Cameron [23]; structure figures were generated with ORTEP-III [24a]. The X-ray diffraction data of ligand and copper complex were collected on an Oxford Diffraction (Agilent Technologies), SuperNova X-ray diffractometer equipped with an Oxford Cryosystems Cobra Low temperature device using  $\text{Cu}-\text{K}\alpha$  radiation ( $\lambda = 1.54184$  &  $1.54178 \text{ \AA}$ ) from a Super Nova Cu X-ray micro source and focusing mirror optics. The structures were solved by direct methods and refined against  $F^2$  by fullmatrix least-squares using the program SHELXTL [24b].

### 2.2. Synthesis of (E)-2-amino-N'-(1-(2-hydroxy-6-methyl-4-oxo-4H-pyran-3-yl)ethylidene)benzo hydrazide ( $\text{H}_2\text{L}$ )

A methanolic solution of *o*-aminobenzoylhydrazide (2 g; 0.01 mol) was added dropwise to a solution of 2-acetyl-5-hydroxy-3-oxo-4-hexenoic acid  $\delta$ -lactone (2.23 g; 0.01 mol) in methanol (20 mL) and the mixture was stirred for 0.5 h at room temperature on mechanical shaker. The progress of the reaction was monitored using TLC. The precipitate formed was filtered off, washed with methanol and then dried *in vacuo*. Pale yellow crystals obtained from slow evaporation of its methanolic solution were suitable for single crystal X-ray diffraction (SC-XRD) analysis. Schematic representation for the synthesis of ligand is given in (Scheme 1).

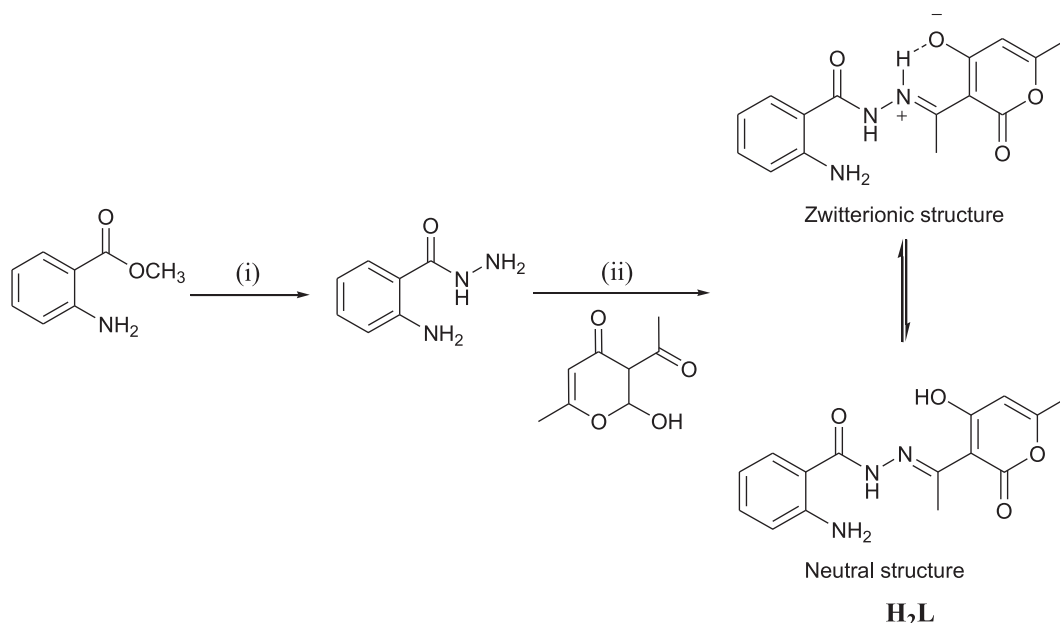
Yield: 87%; m.p.: 193 °C; Color: Pale yellow. Anal. Calcd for  $\text{C}_{15}\text{H}_{15}\text{N}_3\text{O}_4$  (%): C, 59.79; H, 5.02; N, 13.95. Found (%): C, 59.82; H, 4.98; N, 13.92. IR ( $\text{cm}^{-1}$ ):  $\nu = 3323$  (m,  $\text{NH}_2$ , sym.); 3357 (m,  $\text{NH}_2$  asym.); 3447 (m, N–H); 1675 (s, pyranone C=O); 1645 (s, amide C=O); 1619 (m, C=N).  $^1\text{H}$  NMR ( $\text{DMSO}-d_6$ , 400 MHz)  $\delta$ (ppm): 15.90 (s, 1H, O3H), 8.065 (s, 2H, N1H<sub>2</sub>), 5.838 (s, 1H, C11H), 6.772 (d,  $J = 8.4$  Hz, 1H, C4H).  $^{13}\text{C}$  NMR ( $\text{DMSO}-d_6$ , 100 MHz)  $\delta$ (ppm): 162.9 (azomethine C8=N), 170.8 (C7=O), 106.2 (C11H), 16.5 (C14H<sub>3</sub>), 19.2 (C15H<sub>3</sub>).  $\lambda_{\text{max}}$  (nm): 270  $\pi \rightarrow \pi^*$ , 351  $n \rightarrow \pi^*$ .

### 2.3. Synthesis of metal complexes

Methanolic solutions of  $\text{NiCl}_2 \cdot 6\text{H}_2\text{O}$  (0.19 g, 0.8 mmol),  $\text{CuCl}_2 \cdot 2\text{H}_2\text{O}$  (0.14 g, 0.8 mmol) and  $\text{Cu}(\text{CH}_3\text{COO})_2 \cdot \text{H}_2\text{O}$  (0.16 g, 1.6 mmol) were added dropwise to the methanolic solution of  $\text{H}_2\text{L}$  (0.50 g, 1.6 mmol) and stirred for 2 h on mechanical shaker. Co(II) and Zn(II) complexes were obtained by refluxing methanolic solution of  $\text{CoCl}_2 \cdot 6\text{H}_2\text{O}$  (0.19 g, 0.8 mmol) and anhydrous  $\text{ZnCl}_2$  (0.11 g, 0.8 mmol) with methanolic solution of  $\text{H}_2\text{L}$  for 3 h on water bath. The products obtained were filtered off, washed with hot methanol and dried *in vacuo*. Slow evaporation of methanolic solution of Ni(II) complex and DMF solution of Cu (II) complex which was obtained by using  $\text{Cu}(\text{CH}_3\text{COO})_2 \cdot \text{H}_2\text{O}$  salt yielded dark green color single crystals at room temperature suitable for XRD study. Attempts to grow single crystals of the remaining metal complexes were unsuccessful for now.

#### 2.3.1. $[\text{Co}(\text{HL})_2]$

Yield: 52.2%, Color: purple. Anal. Calcd for  $\text{C}_{30}\text{H}_{28}\text{CoN}_6\text{O}_8$  (%): C, 54.63; H, 4.28; N, 12.74; Co, 8.94. Found (%): C, 54.68; H, 4.25; N, 12.78; Co, 8.90. IR ( $\text{cm}^{-1}$ ):  $\nu = 1674$  (s, pyranone C=O); 1620 (s, amide C=O); 1571 (m, C=N).  $\lambda_{\text{max}}$  (nm): 273  $\pi \rightarrow \pi^*$ , 373  $n \rightarrow \pi^*$ , 610 & 674 (d–d transitions). Molar conductivity:  $3.06 \Omega^{-1} \text{ cm}^2 \text{ mol}^{-1}$ .



Reagents and Conditions : (i) NH<sub>2</sub>.NH<sub>2</sub>.H<sub>2</sub>O, MeOH, Reflux (8-9 h)

(ii) MeOH, RT (stirring, 0.5 h)

**Scheme 1.** Synthetic protocol.

### 2.3.2. [Ni(HL)<sub>2</sub>].H<sub>2</sub>O

Yield: 53.6%, Color: green. Anal. Calcd for C<sub>30</sub>H<sub>30</sub>N<sub>6</sub>NiO<sub>9</sub> (%): C, 53.20; H, 4.46; N, 12.41; Ni, 8.67. Found (%): C, 53.16; H, 4.49; N, 12.39; Ni, 8.69. IR (cm<sup>-1</sup>): ν = 1670 (s, pyranone C=O); 1615 (s, amide C=O); 1574 (m, C=N). λ<sub>max</sub>(nm): 274 π → π\*, 395 n → π\*, 554 & 940 (d-d transitions). Molar conductivity: 2.54 Ω<sup>-1</sup> cm<sup>2</sup> mol<sup>-1</sup>.

### 2.3.3. [Cu(HL)<sub>2</sub>]

Yield: 52.8%, Color: dark green. Anal. Calcd for C<sub>30</sub>H<sub>28</sub>CuN<sub>6</sub>O<sub>8</sub> (%): C, 54.26; H, 4.25; N, 12.65; Cu, 9.57. Found(%): C, 54.23; H, 4.21; N, 12.62; Co, 9.53. IR (cm<sup>-1</sup>): ν = 1677 (s, pyranone C=O); 1637 (s, amide C=O); 1599 (m, C=N). λ<sub>max</sub>(nm): 275 π → π\*, 386 n → π\*, 714 (d-d transitions). Molar conductivity: 1.98 Ω<sup>-1</sup> cm<sup>2</sup> mol<sup>-1</sup>.

### 2.3.4. [Zn(HL)<sub>2</sub>]

Yield: 44.8%, Color: Yellow. Anal. Calcd for C<sub>30</sub>H<sub>28</sub>ZnN<sub>6</sub>O<sub>8</sub> (%): C, 51.54; H, 4.97; N, 13.03; Zn, 3.38. Found (%): C, 51.59; H, 4.95; N, 13.07; Zn, 3.41. IR (cm<sup>-1</sup>): ν = 1682 (s, pyranone C=O); 1648 (m, amide C=O); 1590 (m, C=N). <sup>1</sup>H NMR (DMSO-d<sub>6</sub>, 400 MHz) δ(ppm): 6.935 (s, 2H, N1H<sub>2</sub>), 5.737 (s, 1H, C11H), 6.633 (d, J = 8.4 Hz, 1H, C4H). <sup>13</sup>C NMR (DMSO-d<sub>6</sub>, 100 MHz) δ(ppm): 160.1 (azomethine C8=N), 169.6 (C7=O), 107.2 (C11H), 18.9 (C14H<sub>3</sub>), 19.4 (C15H<sub>3</sub>). λ<sub>max</sub>(nm): 276 π → π\*, 384 n → π\*. Molar conductivity: 3.19 Ω<sup>-1</sup> cm<sup>2</sup> mol<sup>-1</sup>.

### 2.3.5. [Cu(L)(H<sub>2</sub>O)]

Yield: 63.4%, Color: green. Anal. Calcd for C<sub>15</sub>H<sub>15</sub>CuN<sub>3</sub>O<sub>5</sub> (%): C, 47.31; H, 3.97; N, 11.03; Cu, 16.69. Found(%): C, 47.28; H, 4.00; N, 11.09; Cu, 16.72. IR (cm<sup>-1</sup>): ν = 1670 (s, pyranone C=O); 1608 (s, amide C=O); 1575 (m, C=N); 1357 (m, C-O). λ<sub>max</sub>(nm): 273 π → π\*, 390 n → π\*, 630 & 635 (d-d transitions). Molar conductivity: 1.98 Ω<sup>-1</sup> cm<sup>2</sup> mol<sup>-1</sup>.

## 2.4. Pharmacology

Ligand and its metal complexes were evaluated for *in vivo* anti-

inflammatory activity by carrageenan-induced rat paw edema model [25,26] and for *in vitro* anti-inflammatory activity by protein denaturation method [27].

### 2.4.1. *In vivo* anti-inflammatory activity: carrageenan-induced rat paw edema model

*In vivo* anti-inflammatory activity was measured as described by Winter et al. [25]. One hour after the administration of the test compounds, the paw edema was induced by injecting 1% carrageenan lambda (a pro-inflammatory agent; prepared in 0.9% NaCl) hypodermically in the sub-plantar region of right hind paw. The test compounds were suspended in 0.5% sodium carboxy methyl cellulose (Na-CMC) and administered at dose of 5 and 10 mg/kg per body weight and declofenac, an anti-inflammatory drug in use was administered orally at a dose of 10 mg/kg, p.o. as the standard. The control group received 0.5% Na-CMC in distilled water. The paw volume was measured at different intervals of time (0.5, 1, 3 and 5 h) using a digital plethysmometer (UGO Basile, Italy), before and after injection of 1% carrageenan lambda. Results were expressed in terms of edema volume as Mean ± SEM and mean percent inhibition according to the following equation,

$$\text{Edema Volume} = V_t - V_c$$

where, V<sub>t</sub> – Paw volume in mL, at time t, after carrageenan administration.

$$V_c - \text{Paw volume in mL, before carrageenan administration}$$

$$\text{Percent inhibition} = E_c - E_t / E_c$$

where, E<sub>c</sub> – Edema volume of rat of control group, at time t.

$$E_t - \text{Edema volume of rat paw, at time t.}$$

**Table 1**  
Selected bond lengths and angles of H<sub>2</sub>L, [Ni(HL)<sub>2</sub>].H<sub>2</sub>O and [Cu(L)DMF].

	H <sub>2</sub> L	[Ni(HL) <sub>2</sub> ].H <sub>2</sub> O	[Cu(L)DMF]
Bond angles (°)			
C7–N2–N3	113.9(10)	115.9(3)	110.4(12)
O1–C7–N2	121.5(11)	121.2(3)	124.5(14)
C8–N3–N2	124.1(10)	119.9(2)	116.7(13)
O2–C11–C10	123.2(11)	125.5(3)	126.1(14)
Bond lengths (Å)			
N1–C1	1.359(17)	1.361(7)	1.382(2)
O1–C7	1.231(15)	1.240(4)	1.299(19)
N2–C7	1.378(15)	1.344(4)	1.318(2)
N2–N3	1.388(14)	1.396(3)	1.396(17)
O2–C11	1.260(15)	1.276(4)	1.281(19)
O4–C15	1.227(15)	1.229(4)	1.217(2)

#### 2.4.2. In vitro anti-inflammatory activity: egg albumin denaturation method

A mixture contained 0.2 mL of egg albumin (from fresh hen's egg), 2.8 mL of phosphate buffered saline (PBS, pH 6.4) and 2 mL of various concentrations of ligand and its metal complexes so that final concentrations become 31.25, 62.5, 125, 250, 500, 1000 µg/mL and similar volume of double-distilled water served as control. Later the mixtures were incubated at (37 ± 2) °C in an incubator (Bio-technics, India) for about 15 min and then heated at 70 °C for 5 min. After cooling, their absorbance was measured at 660 nm (UV-1800 Spectrophotometer, SHIMADZU) by using vehicle as blank. Aceclofenac sodium was used as reference drug and treated similarly for determination of absorbance. The percentage inhibition of protein denaturation was calculated by using the following equation.

$$\% \text{ Inhibition} = 100 \times (\text{Abs of control} - \text{Abs of sample}) / \text{Abs of control}.$$

#### 2.5. Hirshfeld surface analysis

Hirshfeld surfaces (HSs) and 2D fingerprint plots (FPs) were generated using Crystal Explorer 3.1 [28] based on results of SC-XRD studies. The function  $d_{norm}$  is a ratio encompassing the distances of any surface point to the nearest interior ( $d_i$ ) and exterior ( $d_e$ ) atom and the van der Waals radii of the atoms [29a,b,c]. The negative value of  $d_{norm}$  indicates the sum of  $d_i$  and  $d_e$  is shorter than the sum of the relevant van der Waals radii, which is measured to be a closest contact and is visualized as red color in HSs. The white color represents intermolecular distances close to van der Waals contacts with  $d_{norm}$  equal to zero, whereas contacts longer than the sum of van der Waals radii with positive  $d_{norm}$  values are coloured with blue. A plot of  $d_i$  versus  $d_e$  is a 2D fingerprint plot which recognizes the existence of different types of intermolecular interactions.

### 3. Results and discussion

#### 3.1. Single crystal X-ray diffraction and Hirshfeld surface analyses of H<sub>2</sub>L, [Ni(HL)<sub>2</sub>].H<sub>2</sub>O and [Cu(L)DMF]

Summaries of the crystallographic data, selected bond lengths and bond angles of H<sub>2</sub>L, [Ni(HL)<sub>2</sub>].H<sub>2</sub>O and [Cu(L)DMF] are given in Tables S1 and Table 1, respectively. ORTEP representations (asymmetric unit) of the same showing 50% displacement ellipsoids are shown in Figs. 1–3.

The single-crystal X-ray structure of H<sub>2</sub>L was determined at 100 K and is shown to be monoclinic with space group P2<sub>1</sub>/n. Asymmetric unit of H<sub>2</sub>L consists of 3 molecules namely A, B and C with a small trace of crystal held water molecule, (O1W) refines to just under 5% per 3 molecules of H<sub>2</sub>L. These three molecules A, B and C differ marginally from one another in their bond distances and bond angles. Such crystallographically independent and chemically similar molecules are known as bond stretch isomers

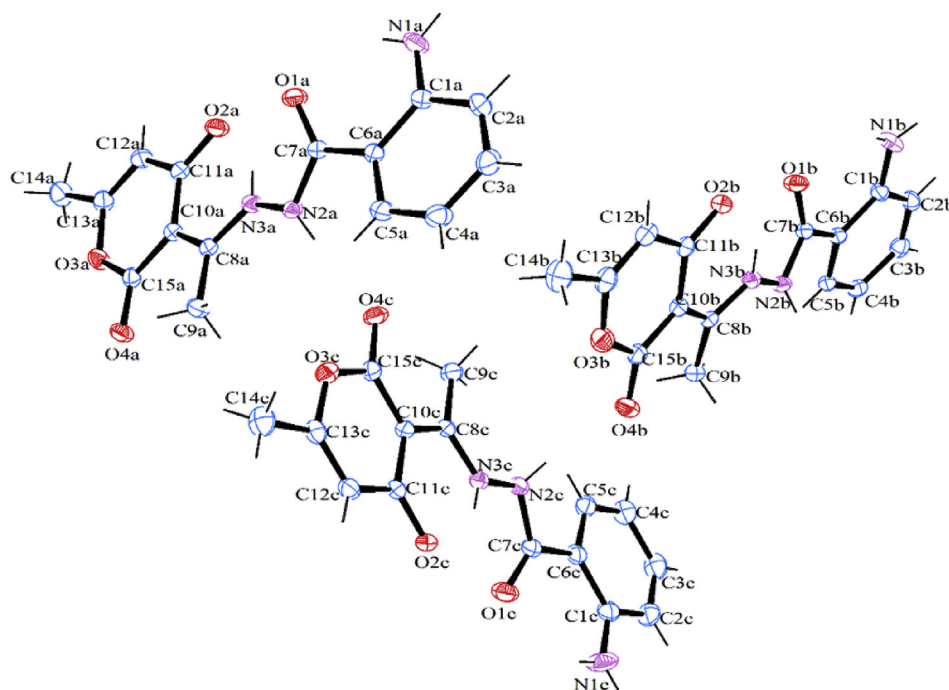


**Fig. 1.** ORTEP projection of H<sub>2</sub>L showing 50% probability ellipsoids.

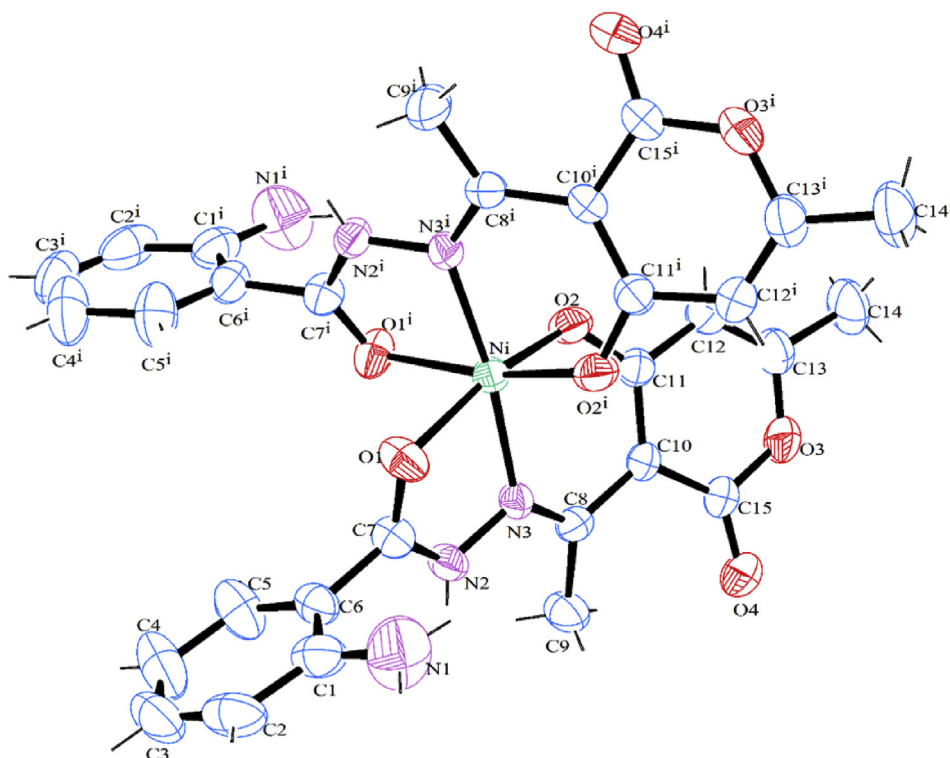


Fig. 2. ORTEP projection of  $[\text{Ni}(\text{HL})_2]\cdot\text{H}_2\text{O}$  showing 50% probability ellipsoids.

[30a,b]. All the three conformers of the ligand is found to exist in zwitterionic form and formally a neutral species as evident by presence of acidic proton (H3AB,H3BB,H3CB) on N3A,N3B,N3C respectively, rather than O2A,O2B,O2C where there exists a single bond character for C11–O2 and double bond character for C8–N3 [30c]. Azomethine and  $>\text{C}=\text{O}$  (mean of O1–C7–N2–N3–C8) form a dihedral angle of  $24.03^\circ$  with the phenyl ring (mean of C1–C6) and  $17.09^\circ$  with DHA ring (mean C10–C11–C12–C13–O3–C15) respectively. Furthermore, the azomethine  $>\text{C}=\text{N}$  bond distance (1.309(16) Å) agrees well with the values for double bond character

confirming the formation of imine bond. The torsion angles  $-3.92(17)$  to  $10.8(17)^\circ$  exhibited by N3–N2–C7–O1,  $-5.41(17)$  to  $11.49(17)^\circ$  by N3–C8–C10–C11 and  $-4.19(18)$  to  $2.10(18)^\circ$  by C8–C10–C11–O2 indicate that N3,O1; N3,C11 and C8,O2 are *cis* to each other respectively, while the torsion angle  $-159.44(12)$  to  $158.01(11)^\circ$  exhibited by C7–N2–N3–C8 indicates that C7 and C8 are *trans* to each other. The structure of  $\text{H}_2\text{L}$  is stabilized by intramolecular N3–H $\cdots$ O2 (2.481(13) Å); N1–H $\cdots$ O1 (2.712(15) Å) and intermolecular N1–H $\cdots$ O2 (2.909(14) Å); N2–H $\cdots$ O4 (2.916(13) Å) hydrogen bonding (Table 2).

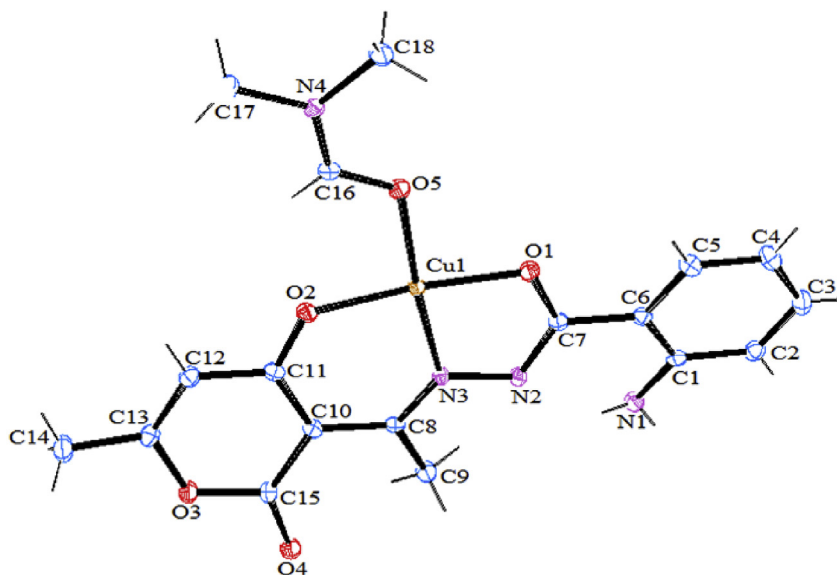


Fig. 3. ORTEP projection of  $[\text{Cu}(\text{L})(\text{DMF})]$  showing 50% probability ellipsoids.

**Table 2**  
Hydrogen bonding (Å, °) in H<sub>2</sub>L, [Ni(HL)<sub>2</sub>].H<sub>2</sub>O and [Cu(L)DMF].

D-H...A <sup>a</sup> interactions	d(D...A)/Å	D-H...A <sup>o</sup>
H <sub>2</sub> L		
N1A-H1AA...O2C <sup>#1</sup>	2.870(14)	170.0(17)
N1A-H1AB...O1A	2.712(15)	132.6(15)
N2A-H2A...O4C	2.764(13)	166.1(15)
N3A-H3AB...O2A	2.481(13)	143.6(17)
N1B-H1BA...O1A <sup>#2</sup>	3.349(16)	152.2(17)
N1B-H1BA...O2A <sup>#2</sup>	2.922(14)	123.3(16)
N1B-H1BB...O1B	2.743(16)	131.9(14)
N2B-H2B...O4A <sup>#3</sup>	2.916(13)	175.3(16)
N3B-H3BB...O2B	2.540(13)	136.6(16)
N1C-H1CA...O2B <sup>#4</sup>	2.935(15)	171.6(18)
N1C-H1CB...O1C	2.733(17)	130.3(17)
N1C-H1CB...O1W <sup>#4</sup>	3.127(10)	147.1(18)
N2C-H2C...O4B	2.804(14)	171.6(16)
N3C-H3CB...O2C	2.515(14)	141.8(16)
[Ni(HL) <sub>2</sub> ].H <sub>2</sub> O		
N1-H1A...O4 <sup>#5</sup>	3.312(5)	149(6)
N1-H1B...Ow	3.207(8)	167(5)
N2-H2A...O4 <sup>#6</sup>	2.978(4)	162(4)
Ow-H5A...O2 <sup>#7</sup>	2.853(4)	142(11)
[Cu(L)DMF]		
N1-H1A...N2	2.691(19)	136.0(2)
N1-H1B...O4 <sup>#8</sup>	2.997(18)	173.0(2)

D: donor; A: acceptor.

<sup>a</sup> Symmetry codes: #1: +X,+Y,-1 + Z; #2: 1/2 - X,-1/2 + Y,1/2 - Z; #3: 1/2 - X,-1/2 + Y,3/2 - Z; #4: +X,+Y,1 + Z; #5: X,-X + Y,1/3 - Z; #6: Y,1 + X,-Z; #7: Y,X - Y,1/3 + Z; #8: X,-Y,1 - Z.

The crystal structure of [Ni(HL)<sub>2</sub>].H<sub>2</sub>O contains 0.5 molecule in the asymmetric unit and structure dimerises across the inversion centre. Hence, results in a pair of tridentate ligands coordinated in *mer* fashion, through an amide carbonyl oxygen, azomethine nitrogen and oxygen of -OH (pyranone ring) via deprotonation. According to International Tables for Crystallography, [Ni(HL)<sub>2</sub>].H<sub>2</sub>O having space group P3<sub>1</sub>, the nickel ion occupies a general position 3a. The bonds Ni-O1(2.082(2) Å), Ni-N3 (2.022(2) Å) and Ni-O2 (1.987(2) Å) forming one five-membered CN<sub>2</sub>ONi and other six-membered C<sub>3</sub>NONi chelate rings with bite angles of 78.75° and 88.08°, respectively, suggest distortion from an ideal octahedral geometry [31]. The bond lengths in [Ni(HL)<sub>2</sub>].H<sub>2</sub>O for: C7-O1 = 1.240(4), N3-C8 = 1.289(4) and C11-O2 = 1.276(4) Å, which are longer or shorter than those of the corresponding distances in the free ligand H<sub>2</sub>L, C7-O1 = 1.231(15), N3-C8 = 1.309(16) and C11-O2 = 1.264(15) Å is due to the coordination of ligand to the central Ni(II) atom. The crystal is stabilized by intramolecular N1-H...Ow (3.207(8) Å) and intermolecular N1-H...O4 (3.312(5) Å); N2-H...O4 (2.978(4) Å); Ow-H...O2 (2.853(4) Å) hydrogen bonding (Table 2). In addition, the molecule is stabilized by intramolecular C-H...π stacking interactions between the centroid of five membered chelate ring and phenyl proton C5-H5, with the contact distance of 3.400 Å and two intermolecular C-H...π stacking interactions, one between the centroid of phenyl ring and proton of DHA ring C12-H14A, another between the centroid of DHA ring and phenyl proton C4-H4, with the contact distances of 3.685 and 3.228 Å respectively (Fig. S1). The C-H...π interactions are important noncovalent intermolecular forces similar to hydrogen bonding.

The single-crystal X-ray structure of [Cu(L)DMF] was determined at 100 K and is shown to be Triclinic with space group P-1. Asymmetric unit of [Cu(L)DMF] consists of one molecule. The crystal structure of [Cu(L)DMF] contains a tridentate ligand coordinated through an amide carbonyl oxygen via deprotonation after enolisation, azomethine nitrogen and oxygen of -OH (pyranone

ring) via deprotonation and also contains a molecule of coordinated DMF. The structure forms a dimer across the inversion centre via a long, (2.685 Å), Cu-N bond. The ONO donor sites of the tridentate ligand coordinate to the Cu(II) centre forming one five-membered CN<sub>2</sub>OCu and other six-membered C<sub>3</sub>NOCu chelate rings with bite angles of 82.98° and 92.10°, respectively, represents distortion from an ideal square planar geometry. The average bond lengths in the complex are: C7-O1 = 1.299(19), N3-C8 = 1.308(2) and C11-O2 = 1.281(19) Å, which are longer or shorter than those of the corresponding distances in the ligand, suggesting considerable delocalization of the charge on the chelate rings [32a]. [Cu(L)DMF] is stabilized by intramolecular hydrogen bonding N1-H...N2 (2.691(19) Å) and also by intermolecular hydrogen bonding N1-H...O4 (2.997(18) Å) (Table 2). In addition, the molecule is stabilized by three intermolecular C-H...π stacking interactions acting between the centroid of chelate ring and phenyl proton C2-H2, the centroid of DHA ring and phenyl protons C2-H2 & C3-H3, with the contact distances of 3.549, 3.758, 3.577 Å respectively (Fig. S2). The π...π interactions can play an important role in packing. In this structure the π...π interaction is an offset stacking, i.e. the rings (DHA and phenyl) are parallel slipped. The ring normal and the vector between the ring centroids form an angle of 20.91° up to centroid-centroid distance of 3.896 Å (Fig. S3) [32b].

Hirshfeld surface analysis is a technique which reproduces the results of X-ray crystal structure analysis and helps to elucidate all the intermolecular interactions in a novel visual manner [33]. This method uses visual recognition of properties of atom contacts through mapping of a range of functions ( $d_{norm}$ , shape index, curvedness, etc.) onto this surface [34]. The increasing popularity of this tool comes from the fact that it allows for recognition of less directional contacts, for instance, H...H dispersion forces. Another essential advantage is that all ( $d_i$ ,  $d_e$ ) contacts created by a molecule of interest can be expressed in the form of a two-dimensional (2D) plot, known as the 2D fingerprint plot. The  $d_e$  and  $d_i$  are defined, respectively, as the distance from the Hirshfeld surface to the nearest atom in the molecule itself and the distance from the surface to the nearest nucleus outwards from the surface. The shape of this plot, which is unique for each molecule, is determined by dominating intermolecular contacts [35]. The Hirshfeld surface mapped with a  $d_{norm}$  function for the H<sub>2</sub>L, [Ni(HL)<sub>2</sub>].H<sub>2</sub>O and [Cu(L)DMF] (Fig. 4a-c) clearly shows the red spots derived from hydrogen bonding interactions. The plots of 2D fingerprint for the H<sub>2</sub>L, [Ni(HL)<sub>2</sub>].H<sub>2</sub>O and [Cu(L)DMF] (Fig. 4a-c) shows the most significant H...H interactions with contribution of 37.9%, 41.8% and 47.0% respectively, other C...H interaction characterized by wing-like peripheral spikes (21.1%, 24.2% and 15.4% respectively), N...H (4.6%, 4.7% and 2.8% respectively) and O...H characterized by longer and thinner spikes (26.3%, 26.7% and 20.9% respectively) (Fig. 4d). The non-directional H...H contacts are characterized by broader spikes in [Cu(L)DMF] and relatively sharper spikes in H<sub>2</sub>L, [Ni(HL)<sub>2</sub>].H<sub>2</sub>O. And, the percentage contribution of H...H contact is also a measure of strength of the crystal lattice [36]. The measurable like volume (VH), area (SH), globularity (G) and asphericity (V) can also be calculated using HSs. The term, globularity [37] is found to be < 1 for H<sub>2</sub>L, [Ni(HL)<sub>2</sub>].H<sub>2</sub>O and [Cu(L)DMF] which indicates that the molecular surface is more structured, not a sphere. The asphericity [38a,b] is a measure of anisotropy which decreases in the ensuing order for the compounds: [Cu(L)DMF] > H<sub>2</sub>L > [Ni(HL)<sub>2</sub>].H<sub>2</sub>O. 2D fingerprint plots of the H<sub>2</sub>L, [Ni(HL)<sub>2</sub>].H<sub>2</sub>O and [Cu(L)DMF] of different intermolecular contacts are displayed in Fig. 4d and Fig. S22.

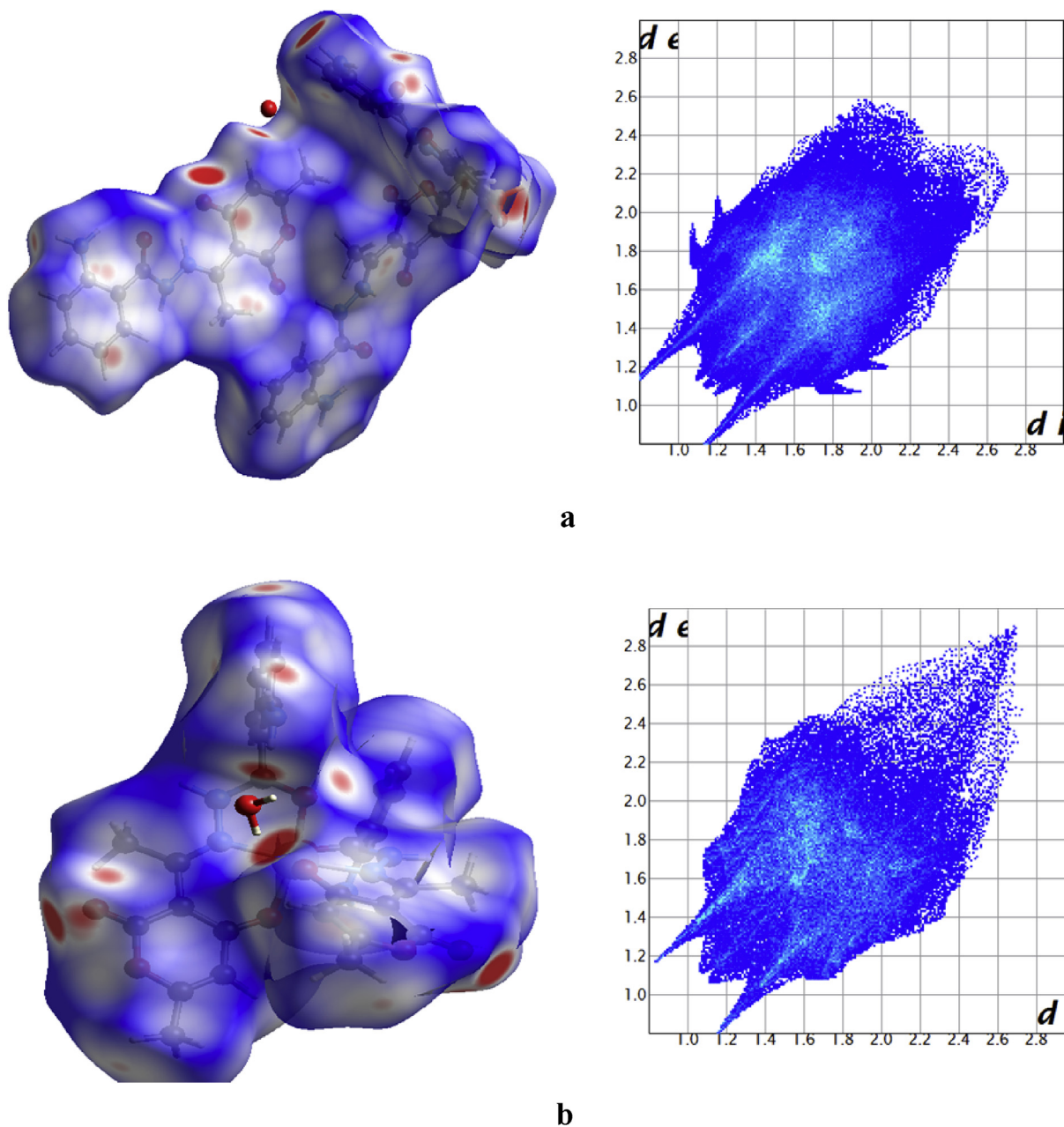


**Fig. 4.** a) Hirshfeld surfaces mapped with *dnorm* and 2D fingerprint plot of H<sub>2</sub>L depicting all intermolecular contributions. b) Hirshfeld surfaces mapped with *dnorm* and 2D fingerprint plot of [Ni(HL)<sub>2</sub>].H<sub>2</sub>O depicting all intermolecular contributions. c) Hirshfeld surfaces mapped with *dnorm* and 2D fingerprint plot of [Cu(L)(DMF)] depicting all intermolecular contributions. d) Distribution of individual intermolecular interactions on the basis of Hirshfeld surface analysis of H<sub>2</sub>L, [Ni(HL)<sub>2</sub>].H<sub>2</sub>O and [Cu(L)(DMF)].

### 3.2. Spectral studies

The IR spectrum of the ligand (H<sub>2</sub>L) showed two highest frequency bands of medium intensity at 3357 and 3323 cm<sup>-1</sup> ascribed to asymmetric and symmetric modes of the ν(-NH<sub>2</sub>) group, respectively. These frequencies have appeared slightly at lower wave number compared to reported compound (2-aminobenzoylhydrazone of 1,3-dione) [39], probably due to the involvement of free amino group in intramolecular hydrogen bonding with the oxygen of C=O of hydrazide moiety as confirmed by crystallographic studies. The presence of symmetric and

asymmetric bands in all the metal complexes due to -NH<sub>2</sub> group indicate the non-involvement of this group in coordination to the metal centers. A medium intense band at 3447 cm<sup>-1</sup> in the free ligand is ascribed to ν(-OH) (pyranone ring). A strong band at 1645 cm<sup>-1</sup> in H<sub>2</sub>L is assigned to amide ν(C=O). This band shows a negative shift in all the complexes except [Cu(L)(H<sub>2</sub>O)] indicating its coordination to the metal ion. The absence of -OH (pyranone ring) stretching band in all the complexes, clearly indicates the involvement of pyranone oxygen in coordination with the metal ion via deprotonation [40]. The strong band at 1619 cm<sup>-1</sup> due ν(C=N) in the ligand has shifted to lower wave number i.e. ~1599 cm<sup>-1</sup> in

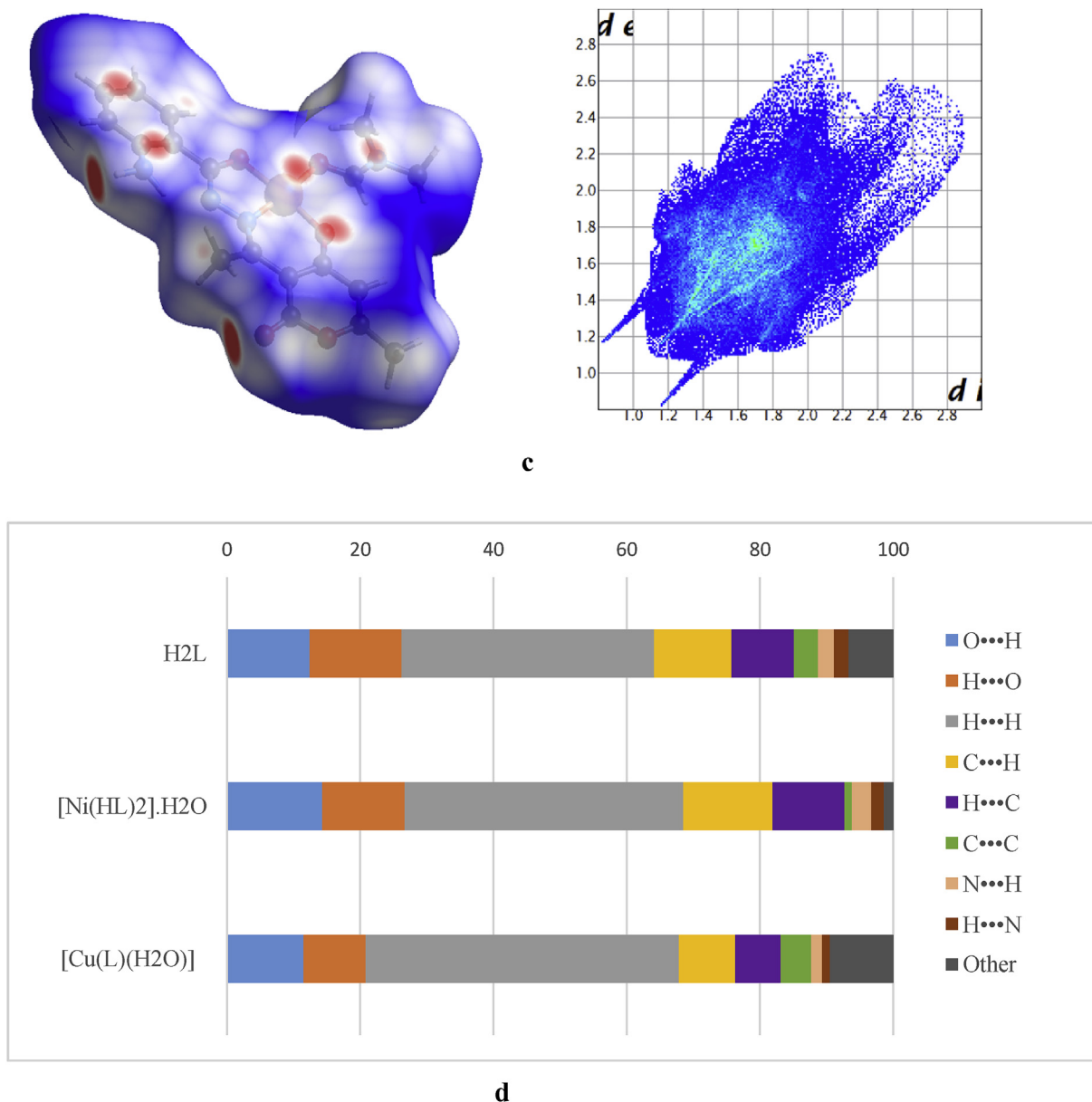


Fig. 4. (continued).

the spectra of all the complexes indicating its coordination to the metal ion. The presence of strong band at  $1675\text{ cm}^{-1}$  assigned to  $\nu(\text{C}=\text{O})$  of pyranone ring in ligand and all the complexes indicates its non-involvement in coordination. The above assignments suggest that the ligand has coordinated through amide carbonyl oxygen, azomethine nitrogen and oxygen of  $-\text{OH}$  group (pyranone ring) via deprotonation in all the complexes except [Cu(L)(H<sub>2</sub>O)]. In case of [Cu(L)(H<sub>2</sub>O)], amide carbonyl stretching  $\nu(\text{C}=\text{O})$  is absent while new bands have been observed at  $1608$  and  $1357\text{ cm}^{-1}$ . These are ascribed to newly formed  $\nu(\text{C}=\text{N})$  and  $\nu(\text{C}-\text{O})$  groups respectively. This indicates the involvement of amide carbonyl oxygen in coordination via enolisation and deprotonation [41a]. Thus, the IR spectral data clearly reveals that the ligand acts as monobasic for all complexes except [Cu(L)(H<sub>2</sub>O)] where it behaves as doubly deprotonated, tridentate ligand. The IR spectra of H<sub>2</sub>L, [Cu(HL)<sub>2</sub>] and [Cu(L)(H<sub>2</sub>O)] (Fig. S4, S5 and S6) are provided as the supplementary

material.

A broad singlet at  $15.76\text{ ppm}$  in the free ligand, ascribed to OH proton has disappeared in the  $^1\text{H}$  NMR spectrum of [Zn(HL)<sub>2</sub>], indicating the coordination of oxygen of  $-\text{OH}$  group (pyranone ring) via deprotonation to the metal ion. A broad singlet at  $8.06\text{ ppm}$  is assigned to two protons of N1. This signal has shifted upfield by  $1.13\text{ ppm}$ , revealing the breakdown of intramolecular hydrogen bonding upon complexation. The signals due to OH proton and two protons of N1 are D<sub>2</sub>O exchangeable (Fig. S8). A singlet appeared at  $5.84\text{ ppm}$  in free ligand ascribed to C12-H corresponds to one proton. A doublet and triplet at  $6.77$  and  $6.57\text{ ppm}$  in free ligand are assigned to C2-H and C4-H, respectively. The aromatic protons resonated as multiplets in the region  $7.57\text{--}7.24\text{ ppm}$  in the spectrum of the free ligand have shifted slightly downfield in the spectrum of [Zn(HL)<sub>2</sub>]. The C9-H<sub>3</sub> and C14-H<sub>3</sub> protons observed as singlets at  $2.11$  and  $2.61\text{ ppm}$  in

uncoordinated ligand have shifted to 2.06 and 2.49 ppm, respectively on complexation. The  $^1\text{H}$  NMR spectra of  $\text{H}_2\text{L}$  (Fig. S7) and  $[\text{Zn}(\text{HL})_2]$  (Fig. S9) are provided as the supplementary material. In the  $^{13}\text{C}$  NMR spectrum of the ligand, the signals at 166.7 and 94.7 ppm correspond to C11 and C9, respectively, and have shifted to 164.4 and 98.0 ppm in the  $^{13}\text{C}$  NMR spectrum of  $[\text{Zn}(\text{HL})_2]$  indicating the coordination of oxygen of  $-\text{OH}$  group (pyranone ring) via deprotonation. The peaks at 162.9, 106.2, 16.5 and 19.2 ppm are assigned to C8, C12, C14 and C9, respectively. The azomethine carbon suffers a downfield shift in the spectrum of  $[\text{Zn}(\text{HL})_2]$  indicating the involvement of azomethine nitrogen in coordination to the metal ion. Methyl carbon C14 also showed a downfield shift in  $[\text{Zn}(\text{HL})_2]$ , indicating the coordination of oxygen of  $-\text{OH}$  group (pyranone ring) via deprotonation to the metal ion. The  $^{13}\text{C}$  NMR spectra of  $\text{H}_2\text{L}$  (Fig. S10) and  $[\text{Zn}(\text{HL})_2]$  are provided as the supplementary material (Fig. S11).  $^1\text{H}$  NMR and  $^{13}\text{C}$  NMR spectra of  $[\text{Zn}(\text{HL})_2]$  suggests coordination of the ligand through oxygen of  $-\text{OH}$  group (pyranone ring) via deprotonation, azomethine nitrogen and amide carbonyl oxygen.

The mass spectrum of the ligand (Fig. S12) has shown the molecular ion peak  $[\text{M}]^+$  at  $m/z$  301. The ESI mass spectra of  $[\text{Co}(\text{HL})_2]$ ,  $[\text{Ni}(\text{HL})_2]\cdot\text{H}_2\text{O}$  and  $[\text{Zn}(\text{HL})_2]$  complexes are given as supplementary material (Fig. S13, S14 and S15). ESI mass spectral studies of  $[\text{Co}(\text{HL})_2]$ ,  $[\text{Ni}(\text{HL})_2]\cdot\text{H}_2\text{O}$ ,  $[\text{Cu}(\text{HL})_2]$ ,  $[\text{Zn}(\text{HL})_2]$  and  $[\text{Cu}(\text{L})(\text{H}_2\text{O})]$  show their molecular ion peaks  $[\text{M}+\text{H}]^+$  at 659, 659,  $[\text{M}+\text{K}]^+$  at 700,  $[\text{M}+\text{Na}]^+$  at 689 and  $[\text{M}+\text{H}]^+$  at 380 respectively. Apart from this, spectra also show some additional peaks, which are due to molecular cations of various fragments of the complexes. By comparing the analytical and spectral data of all the complexes relevant structures were assigned.

The X-band EPR spectra of paramagnetic  $[\text{Cu}(\text{HL})_2]$  complex was measured in the solid state at room temperature and in solution state (DMF) at liquid nitrogen temperature i.e. 77 K. EPR spectra is recorded only for copper complexes, due to the magnetic interactions between the paramagnetic copper centers [41b]. EPR spectra of  $[\text{Cu}(\text{HL})_2]$  are shown in (Fig. S16 and S17). The EPR spectrum at 300 K show a broad absorption band, which is isotropic due to tumbling motion of molecule. The ' $g_{\text{iso}}$ ' value at 300 K is 2.06. The  $g_{\parallel}$  and  $g_{\perp}$  values observed for the complex at 77 K are 2.27 and 2.04, respectively. The trend observed,  $g_{\parallel} > g_{\perp} > 2.02$ , for the present copper complex is typical of a copper (II) ( $d^9$ ) ion in axial symmetry with the unpaired electron residing in  $d_{x^2-y^2}$  orbital [42a,b]. The  $g_{\parallel}$  value ( $2.27 < 2.3$ ) indicates a larger percentage of covalency of metal-ligand bonding [43a]. In axial symmetry the  $g$ -values are related by the expression [43b,c].

$$G = g_{\parallel} - 2/g_{\perp} - 2$$

where,  $G$  is a measure of the exchange interaction between copper centers in the polycrystalline solid. According to Hathway, if the values of the  $G$  are greater than the 4, the exchange interaction is negligible, whereas when the value of  $G$  is less than 4 considerable interaction is indicated in the solid complex [42,43d]. In present investigation the axial symmetry parameter  $G$  being more than 4, rules out the exchange interaction between the copper centers.

### 3.3. Electronic spectral studies

The electronic spectra of the ligand, as well as complexes, were recorded in DMF solvent. The ligand exhibit two absorption bands in the UV–visible region around 270 and 351 nm. The first intense band around 270 nm is assigned to a ligand  $\pi \rightarrow \pi^*$  transition. This band remains almost unchanged in the spectra of all the complexes. The second broad band around 351 nm assigned to  $n \rightarrow \pi^*$

transition, has suffered bathochromic shift upon complexation [44a]. This is an indication of coordination of azomethine nitrogen to the metal ions. For  $[\text{Co}(\text{HL})_2]$ , two spin-allowed transitions observed at 915 and 756 nm were assigned to  $^4\text{T}_{1g}(\text{F}) \rightarrow ^4\text{T}_{2g}(\text{F})$  ( $\nu_1$ ) and  $^4\text{T}_{1g}(\text{F}) \rightarrow ^4\text{A}_{2g}(\text{F})$  ( $\nu_2$ ) transitions indicating an octahedral geometry around  $\text{Co}(\text{II})$  ion [44a,b]. The electronic spectrum of  $[\text{Ni}(\text{HL})_2]\cdot\text{H}_2\text{O}$  displays  $d-d$  transitions around 554 and 940 nm, assignable to  $^3\text{A}_{2g}(\text{F}) \rightarrow ^3\text{T}_{1g}(\text{F})$  ( $\nu_2$ ) and  $^3\text{A}_{2g}(\text{F}) \rightarrow ^3\text{T}_{2g}(\text{F})$  ( $\nu_1$ ) transitions, respectively, indicating an octahedral geometry [45]. A broad band at 714 nm appearing as an envelope in the  $[\text{Cu}(\text{HL})_2]$ , assigned to the  $^2\text{E}_g \rightarrow ^2\text{T}_{2g}$  transition reveals an octahedral geometry [46a,b]. Broad band in the electronic spectrum of  $[\text{Cu}(\text{L})(\text{H}_2\text{O})]$  with peak maxima at 620 nm was assigned to the combination of  $^2\text{B}_{1g} \rightarrow ^2\text{A}_{1g}$  and  $^2\text{B}_{1g} \rightarrow ^2\text{E}_g$  transitions suggest a square-planar configuration around the  $\text{Cu}(\text{II})$  ion [47,48]. The  $\pi \rightarrow \pi^*$ ,  $n \rightarrow \pi^*$  and  $d-d$  transition bands exhibited by the ligand and its metal complexes are shown in Figs. S18 and S19.

### 3.4. Thermal studies

Thermal studies (TG and DT analysis) of all the complexes have been undertaken to know the presence/absence of coordinated/lattice held solvent/water molecules, to confirm their composition and to understand the thermal stability. The thermogram of  $[\text{Ni}(\text{HL})_2]\cdot\text{H}_2\text{O}$  showed a weight loss of 2.70% (Calc. 2.66%) between the temperature range 50 and 100 °C indicating the presence of one lattice held water molecule. This is clearly evidenced in DTA curve in the form of an exothermic peak at 75 °C. Weight loss of 88.82% (Calc. 88.75%) around 200–527 °C corresponds to the loss of two ligand molecules. This process is further supported by two exothermic peaks in DTA curve at 299 and 440 °C. The plateau obtained after heating above 450 °C corresponds to the formation of stable nickel oxide and the metal content (8.60%) calculated from this residue tallies with the metal analysis (8.57%).

$[\text{Co}(\text{HL})_2]$  has remained thermally stable up to a temperature of 200 °C, showing the absence of any lattice held molecules. The weight loss of about 91.70% (Calc. 91.06%) in the range of 200–620 °C is due to the loss of a two ligand molecules. This is clearly evidenced in DTA curve in the form of two exothermic peaks at 276 and 590 °C. The plateau obtained after heating above 600 °C corresponds to the formation of stable cobalt oxide.

The thermogram of  $[\text{Cu}(\text{L})(\text{H}_2\text{O})]$  showing a weight loss of 4.80% (Calc. 4.73%) between the temperature range 180–200 °C correspond to the loss of one coordinated water molecule. Weight loss of 78.76% (Calc. 78.68%) around 250–540 °C correspond to the loss of a ligand molecule. The plateau obtained after heating above 470 °C corresponds to the formation of stable copper oxide. In case of  $[\text{Cu}(\text{HL})_2]$  and  $[\text{Zn}(\text{HL})_2]$  complexes, no weight loss was observed up to the temperature 260 °C and indicates the absence of any lattice held/coordinated solvent molecule. The weight loss of 85.27 and 90.03% (Calc. 85.22% and 90.22%) around 265–650 °C correspond to the loss of two ligand molecule. Weight of the residue obtained after heating the complex above 650 °C corresponds to the formation of stable metal oxides.

Thus, thermal studies support the suggested composition for the complexes. As representatives, thermograms of  $[\text{Ni}(\text{HL})_2]\cdot\text{H}_2\text{O}$  and  $[\text{Co}(\text{HL})_2]$  are given in Figs. S20 and S21 respectively.

### 3.5. Anti-inflammatory activity

In the present investigation, the control group showed a significant increase of edema in the right hind paw of the animals in the plantar region. This is due to the release of inflammatory mediators such as histamine, serotonin, kinins, and prostaglandins

**Table 3**  
*In vivo* anti-inflammatory activity of H<sub>2</sub>L and its metal complexes.

Treatment	0.5 h		0.5 h		3 h		5 h	
	Paw volume (ml)	% EI						
Control	1.097 ± 0.04356	—	1.197 ± 0.01411	—	1.170 ± 0.06208	—	1.343 ± 0.02789	—
Diclofenac (10 mg kg <sup>-1</sup> )	0.0300 ± 0.0267***	97.2	0.0300 ± 0.0267***	97.26	0.1083 ± 0.0401***	90.74	0.0250 ± 0.0125***	98.13
H <sub>2</sub> L(5 mg kg <sup>-1</sup> )	0.2839 ± 0.0264***	90.02	0.1686 ± 0.0184***	65.26	0.7464 ± 0.0173***	41.28	0.2975 ± 0.0154***	88.26
H <sub>2</sub> L(10 mg kg <sup>-1</sup> )	0.2481 ± 0.0326***	87.20	0.1745 ± 0.0326***	69.25	0.8453 ± 0.0275***	40.08	0.4245 ± 0.0163***	93.54
[Co(HL) <sub>2</sub> ] (5 mg kg <sup>-1</sup> )	0.2965 ± 0.0256***	92.01	0.1384 ± 0.0102***	69.32	0.7675 ± 0.0162***	76.25	0.5964 ± 0.0142***	83.25
[Co(HL) <sub>2</sub> ] (10 mg kg <sup>-1</sup> )	0.2665 ± 0.0146***	89.84	0.1013 ± 0.0115***	84.71	0.5543 ± 0.0156***	71.92	0.3520 ± 0.0142***	94.65
[Ni(HL) <sub>2</sub> ].H <sub>2</sub> O (5 mg kg <sup>-1</sup> )	0.3954 ± 0.0164***	85.58	0.1895 ± 0.0164***	71.92	0.9732 ± 0.0334***	63.25	0.6784 ± 0.0353***	84.12
[Ni(HL) <sub>2</sub> ].H <sub>2</sub> O (10 mg kg <sup>-1</sup> )	0.2265 ± 0.0167***	82.98	0.1035 ± 0.0154***	78.63	0.6924 ± 0.0143***	53.69	0.3521 ± 0.0321***	88.97
[Cu(HL) <sub>2</sub> ] (5 mg kg <sup>-1</sup> )	0.2937 ± 0.0264***	87.23	0.1546 ± 0.0153***	76.02	0.7455 ± 0.0245***	22.22	0.6342 ± 0.0245***	82.25
[Cu(HL) <sub>2</sub> ] (10 mg kg <sup>-1</sup> )	0.2367 ± 0.0232***	89.55	0.1014 ± 0.0176***	79.02	0.5234 ± 0.0257***	36.52	0.5321 ± 0.0165***	89.25
[Zn(HL) <sub>2</sub> ] (5 mg kg <sup>-1</sup> )	0.4673 ± 0.0265***	85.03	0.2675 ± 0.0164***	76.25	0.5743 ± 0.0143***	64.59	0.5143 ± 0.0164***	96.52
[Zn(HL) <sub>2</sub> ] (10 mg kg <sup>-1</sup> )	0.3856 ± 0.0156***	86.66	0.1675 ± 0.0168***	80.25	0.5325 ± 0.0156***	62.82	0.2532 ± 0.0153***	92.52
[Cu(L)(H <sub>2</sub> O)] (5 mg kg <sup>-1</sup> )	0.2464 ± 0.0267***	95.21	0.2015 ± 0.0273***	81.25	0.7833 ± 0.0174***	39.25	0.3125 ± 0.0162***	79.52
[Cu(L)(H <sub>2</sub> O)] (10 mg kg <sup>-1</sup> )	0.2318 ± 0.0356***	93.21	0.1945 ± 0.0183***	85.26	0.7845 ± 0.0126***	42.35	0.2967 ± 0.0144***	85.53

All values are expressed as mean SEM, ANOVA followed by Dunnett's test.

\*\*P < 0.01 and \*\*\*P < 0.001 as comparison of test groups to control group.

(PGs). The edema development after carrageenan injection has been described as a biphasic event in which various mediators operate in sequence to produce this inflammatory response. The initial phase of edema (0–1 h), which is not inhibited by non-steroidal anti-inflammatory drugs, has been attributed to the release of histamine, 5-hydroxytryptamine (5-HT) and bradykinin.

In contrast, the second accelerating phase of swelling (1–6 h), has been correlated with the elevated production of prostaglandins [49], and more recently has been attributed to the induction of inducible cyclo-oxygenase (COX-2) in the hind paw. Local neutrophil infiltration and activation also contribute to this inflammatory response by producing, among other mediators, oxygen-derived free radicals such as superoxide anion (O<sup>2-</sup>) and hydroxyl radicals. Among them, edema is one of the most fundamental actions of acute inflammation and is an essential parameter to be considered when evaluating compounds with potential anti-inflammatory activities [50a].

The coordination of bioactive molecules to metal ions is a promising approach to improve the therapeutic potency and/or to decrease the toxicity of drug molecules. The resulting metal complexes possess greater lipophilicity profiles compared to the free ligands, allowing them to more easily pass through cell membranes to exert their biological effects [8b,c].

### 3.5.1. *In vivo* anti-inflammatory activity

The anti-inflammatory activity of the newly synthesized compounds were evaluated by applying the carrageenan-induced paw edema bioassay in rats using diclofenac as reference drug [50b–d]. In the present investigation, the ligand and its metal complexes exhibited a dose-dependent response (Table 3). The ligand, H<sub>2</sub>L showed a consistent and significant decrease in paw edema at 0.5, 1, 3 and 5 h after drug administration, while complexes at higher dose gave a good response up to the fifth hour but at a lower dose, the significant response decreased as time advanced. Further, the copper complexes ([Cu(HL)<sub>2</sub>] and [Cu(L)(H<sub>2</sub>O)]) showed significant inhibition of paw edema at a lower concentration of 5 mg/kg. The percentage inhibition (22–82%) shown by [Cu(HL)<sub>2</sub>] over the time period of 0.5–1 h was significant and comparable with the standard compound, viz. Diclofenac (90–98%) (Fig. 5a–b). In comparison with H<sub>2</sub>L, all the complexes showed excellent effect at 0.5 and 1 h, [Co(HL)<sub>2</sub>], [Zn(HL)<sub>2</sub>] and [Cu(L)(H<sub>2</sub>O)] retained their activity up to fifth hour, while [Ni(HL)<sub>2</sub>].H<sub>2</sub>O and [Cu(HL)<sub>2</sub>] showed a gradual decrease in activity. The enhanced anti-inflammatory activity of the complexes compared to the free ligand may be explained on the basis of enhanced pervasion through cellular membrane on complexation by Tweedy's Chelation theory and Overton's concept [51a]. According to Overton's concept of cell permeability, the lipid membrane that surrounds the cell favors the passage of only the lipid-soluble materials in which liposolubility as an important factor, which controls the biological activity. On

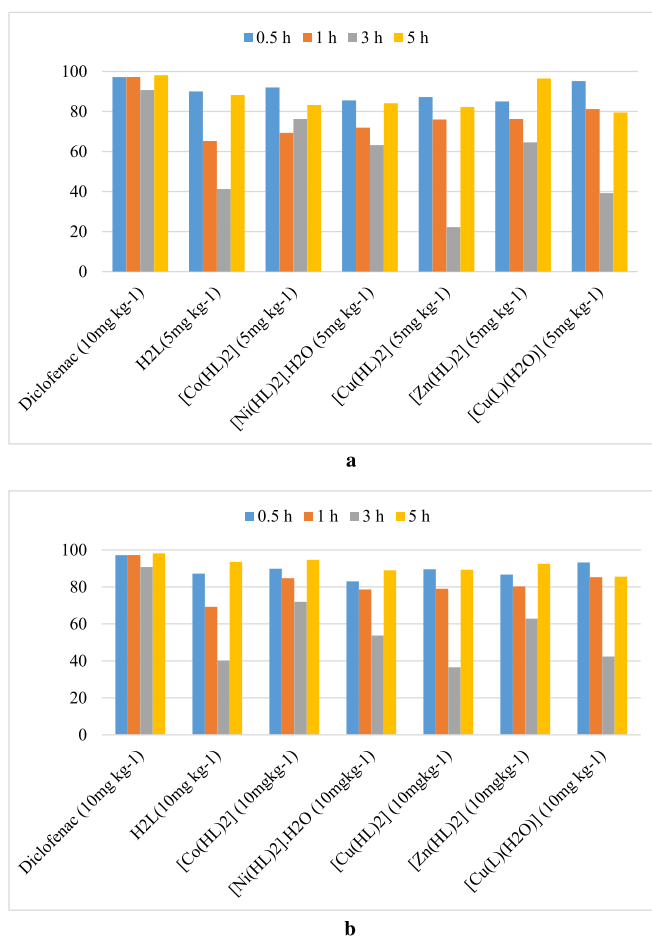


**Fig. 5.** a) Anti-inflammatory activity of H<sub>2</sub>L and its metal complexes at different time intervals (0.5–5 h) with 5 mg/kg dose. b) Anti-inflammatory activity of H<sub>2</sub>L and its metal complexes at different time intervals (0.5–5 h) with 10 mg/kg dose.

**Table 4**  
*In-vitro* anti-inflammatory activity of H<sub>2</sub>L and its metal complexes.

Entry	Metal	% Inhibition of egg albumin in 250 µg/mL
Acetoclofenac	–	43.2
H <sub>2</sub> L	–	33.9
[Co(HL) <sub>2</sub> ]	Co	34.8
[Ni(HL) <sub>2</sub> ].H <sub>2</sub> O	Ni	80.6
[Cu(HL) <sub>2</sub> ]	Cu	55.3
[Zn(HL) <sub>2</sub> ]	Zn	45.3
[Cu(L)(H <sub>2</sub> O)]	Cu	38.4

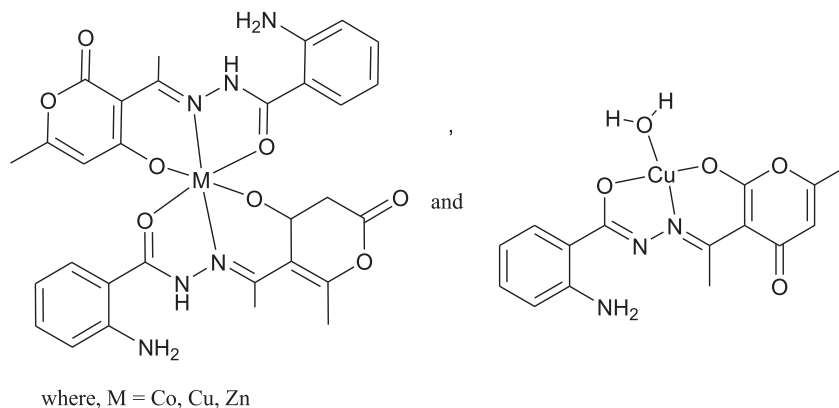


**Fig. 6.** Tentatively proposed structures of [Co(HL)<sub>2</sub>], [Cu(HL)<sub>2</sub>], [Zn(HL)<sub>2</sub>] and [Cu(L)(H<sub>2</sub>O)].

chelation, the polarity of the metal ion will be reduced due to the overlap of the ligand orbital and partial sharing of the positive charge of the metal ion with donor groups [51b]. It is also expected that the more extensive heteroaromatic ring like DHA and the presence of lipophilic group C=N would bestow greater lipophilicity on complexes and enable it to penetrate the cell wall and promote adverse intracellular interactions [51c]. Hence, the enhanced activity of the complexes can be related to reduced overall polarity of the molecule, which increases the lipophilic nature of the complex, favoring the efficient permeation through lipid layer.

### 3.5.2. *In vitro* anti-inflammatory activity

*In vitro* pharmacological evaluation of the title compounds was carried out to evaluate their anti-inflammatory activity. All the synthesized compounds were subjected to anti-inflammatory effect against denaturation of hen's egg albumin method [52a,b] at the concentration (31.25–1000 µg/mL) with standard acetoclofenac drug. The outcome of anti-inflammatory screening of the title compounds are summarized in Table 4. The percentage inhibition of all the synthesized compounds showed higher activity against the denaturation of protein. Among the compounds, [Ni(HL)<sub>2</sub>].H<sub>2</sub>O, [Cu(HL)<sub>2</sub>] and [Zn(HL)<sub>2</sub>] exhibited an excellent inhibition of heat induced protein denaturation 80.6%, 55.3% and 45.3% respectively and these compounds are more active compared to standard acetoclofenac drug (43.2%). All the metal complexes showed good inhibitory anti-inflammatory activity than the free ligand against the denaturation of the protein.

## 4. Conclusion

In the present work, Co(II), Ni(II), Cu(II) and Zn(II) complexes of a new ligand, (*E*)-2-amino-*N'*-(1-(2-hydroxy-6-methyl-4-oxo-4H-

pyran-3-yl)ethylidene) benzohydrazide were designed and synthesized in good yield. Analytical and spectroscopic data for the metal complexes indicate a 1:1 (M: L) stoichiometry for [Cu(L)(H<sub>2</sub>O)] adopting a square planar geometry and 1:2 for the [Co(HL)<sub>2</sub>], [Ni(HL)<sub>2</sub>].H<sub>2</sub>O, [Cu(HL)<sub>2</sub>] and [Zn(HL)<sub>2</sub>] adopting an octahedral geometry around the metal ion. The organic motif, H<sub>2</sub>L coordinated in monoanionic i.e. coordinating through oxygen of –OH group (pyranone ring) via deprotonation in [Co(HL)<sub>2</sub>], [Ni(HL)<sub>2</sub>].H<sub>2</sub>O, [Cu(HL)<sub>2</sub>], [Zn(HL)<sub>2</sub>] and in dianionic form i.e. deprotonation after enolisation of amide carbonyl & deprotonation of –OH group (pyranone ring) in [Cu(L)(H<sub>2</sub>O)]. Thus, the ligand acts

in mono as well as doubly deprotonated manner. The tentative structures for metal complexes are depicted in Fig. 6. All interactions in crystal structures of H<sub>2</sub>L, [Ni(HL)<sub>2</sub>].H<sub>2</sub>O and [Cu(L)DMF] have also been studied by Hirshfeld surface analysis. H<sub>2</sub>L and its metal complexes have also been screened for their *in vivo* and *in vitro* anti-inflammatory activities. The results showed that activity of ligand has enhanced on complexation. The increase in activity of the metal complexes is probably due to the greater lipophilic nature of the complexes. Among the complexes tested, [Cu(HL)<sub>2</sub>] has shown highest activity. The difference in activity among the tested compounds may be attributed to the electrostatic nature of ligand and central metal ion.

## 5. Significance and justification

The present research reports *in vivo* and *in vitro* anti-inflammatory activity of late first row transition metal complexes of novel ligand. The results showed that activity of ligand has enhanced on complexation. The results of the present study are quite inspiring and warrant further, extensive testing toward transfer into the clinical arena.

## Acknowledgements

Authors thank USIC, Karnatak University, Dharwad for IR spectral analyses, TGA and SC-XRD studies and CDRI Lucknow for ESI mass analyses. Recording of <sup>1</sup>H and <sup>13</sup>C NMR spectra from IISC-Bangalore and EPR spectra from IIT-Bombay are gratefully acknowledged. Authors are also thankful to Dr. M. Netaji for his help in solving the crystal data of Nickel complex. One of the author, Geeta H. Chimmalagi acknowledges UGC for providing RFSMS scholarship.

## Appendix A. Supplementary data

Supplementary data related to this article can be found at <https://doi.org/10.1016/j.molstruc.2017.10.022>.

## References

- [1] M.V. Angelusiu, S.F. Barbuceanu, C. Draghici, G.L. Almajan, *Eur. J. Med. Chem.* 45 (2010) 2055–2062.
- [2] S. Naskar, S. Naskar, R.J. Butcher, S.K. Chattopadhyay, *Inorg. Chim. Acta* 363 (2010) 404–411.
- [3] H.G. Aslan, S. Ozcan, N. Karacan, *Inorg. Chem. Commun.* 14 (2011) 1550–1553.
- [4] (a) Q. Wang, Z.Y. Yang, G.F. Qi, *BioMetals* 22 (2009) 927–940; (b) Z. Xu, X. Zhang, W. Zhang, Y. Gao, Z. Zeng, *Inorg. Chem. Commun.* 14 (2011) 1569–1573.
- [5] S. Rollas, S.G. Küçükgülzel, *Molecules* 12 (2007) 1910–1939.
- [6] M. Caacelli, P. Mazza, C. Pelizzi, G. Pelizzi, F. Zani, *J. Inorg. Biochem.* 57 (1995) 43–62.
- [7] S. Banerjee, S. Mondal, W. Chakraborty, S. Sen, R. Gachhui, R.J. Butcher, A.M.Z. Slawin, C. Mandal, S. Mitra, *Polyhedron* 28 (2009) 2785–2793.
- [8] (a) V.P. Singh, S. Singh, D.P. Singh, *J. Enz. Inhib. Med. Chem.* 27 (2012) 319–329; (b) Chung-Hang Leung, S. Lin, Hai-Jing Zhong, Dik-Lung Ma, *Chem. Sci.* 6 (2015) 871–884; (c) R.S. Hoonur, B.R. Patil, D.S. Badiger, R.S. Vadavi, K.B. Gudasi, P.R. Dandawate, M.M. Ghaisas, S.B. Padhye, M. Nethaji, *Eur. J. Med. Chem.* 45 (2010) 2277–2282.
- [9] S.R. Thomas, K.D. Janda, *J. Am. Chem. Soc.* 122 (2000) 6929–6934.
- [10] H.H. Monfared, S. Sadighian, M.A. Kamyabi, P. Mayer, *J. Mol. Catal. A Chem.* 304 (2009) 139–146.
- [11] Y. Nakayama, H. Bando, Y. Sonobe, T. Fujita, *J. Mol. Catal. A Chem.* 213 (2004) 141–150.
- [12] D.P. Singh, D.S. Raghuvanshi, K.N. Singh, V.P. Singh, *J. Mol. Catal. A Chem.* 379 (2013) 21–29.
- [13] A. Ourari, W. Derafa, D. Aggoun, *RSC Adv.* 5 (2015) 82894–82905.
- [14] E.S. Azam, A.F. EL-Husseiny, H.M. Al-Amri, *Arab. J. Chem.* 5 (2012) 45–53.
- [15] T. Punniyamurthy, S.J.S. Kalra, J. Iqbal, *Tett. Lett.* 36 (1995) 8497–8500.
- [16] (a) P.N.P. Rao, M. Amini, Li Huiying, A.G. Habeeb, E.D. Knaus, *Bioorg. Med. Chem. Lett.* 13 (2003) 2205–2209; (b) M.R. Maurya, N. Saini, F. Aveccilla, *Polyhedron* 90 (2015) 221–232; (c) N. Chitrapriya, V. Mahalingam, M. Zeller, K. Natarajan, *Inorg. Chim. Acta* 363 (2010) 3685–3693; (d) Fathy A. El-Saied, Ahmed A. El-Asmy, Werner Kaminsky, Douglas X. West, *Transit. Met. Chem.* 28 (2003) 954–960; (e) S. Karamouzi, A. Maniadaki, D.A. Nasiopoulou, E. Kotali, A. Kotali, P.A. Harris, J. Raftery, J.A. Joule, *Synthesis* 45 (2013) 2150–2154; (f) T. Mangamamba, M.C. Ganorkar, G. Swarnabala, *Int. J. Inorg. Chem.* (2014) 1–22; (g) A. Kotali, F. Dimoulaki, E. Kotali, A. Maniadaki, P.A. Harris, E. Rózycka-Sokotowska, P. Batczewski, J.A. Joule, *Tetrahedron* (2015) 1–5; (h) S. Liu, S.J. Rettig, C. Orvig, *Inorg. Chem.* 30 (1991) 4915–4919.
- [17] P. Krishnamoorthy, P. Sathyadevi, R.R. Butorac, A.H. Cowley, Nattamai, S.P. Bhuvanesh, N. Dharmaraj, *Dalton Trans.* 41 (2012) 4423–4436.
- [18] R.N. Pandey, A.N. Sahay, P. Sharma, S. Kumar, A.K. Pathak, *Asian J. Chem.* 6 (1994) 747–752.
- [19] G.P.A. Yap, I. Alkorta, N. Jagerovic, J. Elguero, *Aust. J. Chem.* 57 (2004) 1103–1108.
- [20] A.I. Vogel, *A Textbook of Quantitative Inorganic Analysis*, third ed., Longmans Green and Co. Ltd, London, 1961.
- [21] R.I. Cooper, A.L. Thompson, D.J. Watkin, *J. Appl. Cryst.* 43 (2010) 1100–1107.
- [22] P.W. Betteridge, J.R. Carruthers, R.I. Cooper, K. Prout, D.J. Watkin, *J. Appl. Cryst.* 36 (2003), 1487–1487.
- [23] D.J. Watkin, C.K. Prout, L.J. Pearce, CAMERON, *Chemical Crystallography Laboratory*, Oxford, England, 1996.
- [24] (a) M.N. Burnett, C.K. Johnson, ORTEP-III: Oak Ridge Thermal Ellipsoid Plot Program for Crystal Structure Illustrations, Oak Ridge National Laboratory Report ORNL-6895, 1996; (b) G.M. Sheldrick, SHELXTL Version 5.0, Bruker AXS Inc., Madison, Wisconsin, USA, 2001.
- [25] C.A. Winter, E.A. Riskey, G.W. Nuss, *Proc. Soc. Exp. Biol. Med.* 111 (1962) 544–552.
- [26] P. Kumar, E.E. Knaus, *Drug Des. Deliv.* 2 (1987) 145–149.
- [27] S.R. Devineni, M. Golla, N.R. Chamarthi, B. Meriga, M.S. Saddala, S.R. Asupathri, *Med. Chem. Res.* 25 (2016) 751–768.
- [28] S.K. Wolff, D.J. Grimwood, J.J. McKinnon, M.J. Turner, D. Jayatilaka, M.A. Spackman, *Crystal Explorer 3.1*, University of Western Australia, Crawley, Western Australia, 2013, pp. 2005–2013.
- [29] (a) M.A. Spackman, J.J. McKinnon, *Cryst. Eng. Comm.* 4 (2002) 378–392; (b) F.L. Hirshfeld, *Theor. Chim. Acta* 44 (1977) 129–138; (c) M.A. Spackman, D. Jayatilaka, *Cryst. Eng. Comm.* 11 (2009) 19–32.
- [30] (a) K.K. Narang, U.S. Yadav, *Ind. J. Chem.* 19A (1979) 697–700; (b) K.K. Narang, U.S. Yadav, *Ind. J. Chem.* 20A (1981) 404–405; (c) A. Djedouani, A. Bendaas, S. Boufas, M. Allain, G. Bouetd, M. Khand, *Acta Cryst. E* 63 (2007) 1271–1273.
- [31] R. Shakya, C. Imbert, H.P. Hratchian, M. Lanznaster, M.J. Heeg, B.R. McGarvey, M. Allard, H.B. Schlegel, C.N. Verani, *Dalton Trans.* 21 (2006) 2517–2525.
- [32] (a) J.R. Dilworth, J. Hyde, P. Lyford, P. Vella, K. Venkatasubraman, J.A. Zubieta, *Inorg. Chem.* 18 (1979) 268–274; (b) C. Janiak, *J. Chem. Soc. Dalton Trans.* (2000) 3885–3896.
- [33] A.M. Spackman, D. Jayatilaka, *Cryst. Eng. Comm.* 11 (2009) 19–32.
- [34] J.J. Mac Kimon, M.A. Spackman, A.S. Mitchell, *Acta Cryst. B* 60 (2004) 627–668.
- [35] J.J. MacKimon, D. Jayatilaka, A.M. Spackman, *Chem. Commun.* 37 (2007) 3814–3816.
- [36] S. Grabowsky, P.M. Dean, B.W. Skelton, A.N. Sobolev, M.A. Spackman, A.H. White, *Cryst. Eng. Comm.* 14 (2012) 1083–1093.
- [37] A.Y. Meyer, *Chem. Soc. Rev.* 15 (1986) 449–474.
- [38] (a) J. Rudnick, G. Gaspari, *J. Phys. A Math. Gen. Phys.* 19 (1986) L191–L193; (b) A. Baumgartner, *J. Chem. Phys.* 99 (1993) 7496–7501.
- [39] J. Barleunga, L.A. Lopez, S. Martinez, M. Tomas, *Synlett* 2 (1999) 219–221.
- [40] N. Chitrapriya, T.S. Kamatchi, M. Zeller, H. Lee, K. Natarajan, *Spectrochim. Acta. A* 81 (2011) 128–134.
- [41] (a) R.S. Hunoor, B.R. Patil, D.S. Badiger, V.M. Chandrashekar, I.S. Muchchandi, K.B. Gudasi, *Appl. Organomet. Chem.* 29 (2015) 101–108; (b) A. Winter, K. Thiel, A. Zabel, T. Klamroth, A. Pöpl, A. Kelling, U. Schilde, A. Taubert, P. Strauch, *New J. Chem.* 38 (2014) 1019–1030.
- [42] (a) Syamal, R.L. Dutta, *Elementals of Magneto Chemistry*, East–West Press Pvt. Ltd., New Delhi, 2004; (b) K.M. Vyas, R.N. Jadej, V.K. Gupta, K.R. Surati, *J. Mol. Struct.* 990 (2011) 110–120.
- [43] (a) D. Kivelson, R. Neiman, *J. Chem. Phys.* 35 (1961) 149–155; (b) B. Bottaria, R. Maccaria, F. Monforte, R. Ottanà, E. Rotondo, M.G. Vigorita, *Bioorg. Med. Chem. Lett.* 11 (2001) 301–303; (c) B. Bottaria, R. Maccaria, F. Monforte, R. Ottanà, E. Rotondo, M.G. Vigorita, *Bioorg. Med. Chem. Lett.* 10 (2000) 657–660; (d) R.J. Dudley, B.J. Hathaway, *J. Chem. Soc. A* (1970) 1725–1728.
- [44] (a) V. Kamat, D. Kokare, K. Naik, A. Kotian, S. Naveen, S.R. Dixit, N.K. Lokanath, S.D. Joshi, V.K. Revankar, *Polyhedron* 127 (2017) 225–237; (b) N. Sathyanarayana, *Electronic Absorption Spectroscopy and Related Techniques*, University Press (India) Limited, Hyderabad, 2001.
- [45] A.B.P. Lever, *Inorganic Electronic Spectroscopy*, second ed., Elsevier, Amsterdam, 1984.
- [46] (a) J.C. Bailar, H.J. Emeleus, S.R. Nyholm, A.F.T. Dickenson, *Comprehensive Inorganic Chemistry*, Pergamon Press, Oxford, 1975; (b) K.B. Gudasi, S.A. Patil, R.S. Vadavi, R.V. Shenoy, M.S. Patil, M. Netaji, *Trans. Met. Chem.* 31 (2006) 586–592.
- [47] H.O.J. Collier, L.C. Dinneen, C.A. Johnson, C. Schneider, *Br. J. Pharmacol.* 32 (1968) 295–310.
- [48] K. Vinay, A.K. Abul, F. Nelson, Mitchell, N. Rechar, Robbins *Basic Pathology*, eighth ed., Saunders Elsevier, 2007, pp. 516–522.
- [49] M.D. Rosa, J.P. Giroud, D.A. Willoughby, *J. Pathol.* 104 (1971) 15–29.
- [50] (a) C.J. Morris, *Meth. Mol. Biol.* 225 (2003) 115–121; (b) M. Jesmin, M.K. Islam, S.M.M. Ali, *Int. Lett. Chem. Phys. Astron.* 27 (2014) 64–72; (c) S.D. Narayanachar, S. Dhumwad, M.H. Mutalik, P.N. Hugar, Naik, Main. *Group Chem.* 12 (2013) 87–104; (d) R. Shanmugakala, P. Tharmaraj, C.D. Sheela, N. Chidambaranathan, *Med. Chem. Res.* 23 (2014) 329–342.
- [51] (a) B.G. Tweedy, *Phytopathology* 55 (1964) 910–914; (b) T.D. Thangadurai, K. Natarajan, *Transit. Met. Chem.* 26 (2001) 500–504; (c) J. Joseph, K. Nagashri, G.A.B. Rani, *J. Saudi Chem. Soc.* 17 (2013) 285–294.
- [52] (a) S.R. Devineni, M. Golla, N.R. Chamarthi, B. Meriga, M.S. Saddala, S.R. Asupathri, *Med. Chem. Res.* 25 (2016) 751–768; (b) B.M. Chougala, S. Samundeeswari, M. Holiyachi, L.A. Shastri, S. Dodamani, S. Jalalpure, S.R. Dixit, S.D. Joshi, V.A. Sunagar, *Eur. J. Med. Chem.* 125 (2017) 101–116.